Title

Application of the fluctuation theorem for non-invasive force measurement in living neuronal axons.

Authors

Kumiko Hayashi [1 *], Yuta Tsuchizawa [2,3], Mitsuhiro Iwaki [4], Yasushi Okada [2, 5, *]

Affiliations

[1]Department of Applied Physics, Graduate School of Engineering, Tohoku University, Sendai, Japan

[2]Laboratory for Cell Polarity Regulation, Quantitative Biology Center, RIKEN, Osaka, Japan

[3]Graduate School of Frontier Biosciences, Osaka University, Osaka, Japan

[4]Laboratory for Cell Dynamics Observation, Quantitative Biology Center, RIKEN, Osaka, Japan

[5]Department of Physics and Universal Biology Institute, Graduate School of Science, The University of Tokyo, Tokyo, Japan

*Correspondence: kumiko@camp.apph.tohoku.ac.jp (K.H.), y.okada@riken.jp (Y.O.)

Abstract

Although its importance is widely accepted recently, force measurement has been difficult in living biological systems, mainly due to the lack of the versatile non-invasive force measurement methods. The fluctuation theorem, which represents the thermodynamic properties of small fluctuating non-equilibrium systems, has been applied to the analysis of the thermodynamic properties of motor proteins *in vitro*. Here, we extend it to the axonal transport of endosomes. The fluctuation of their displacement distributed with several distinct peaks at multiples of a unit value, which the fluctuation theorem can convert into the drag force exerted on the endosomes. The results demonstrated that a single cargo vesicle is often conveyed by two to three force producing units. Furthermore, this method enabled us to compare the force-velocity relations *in vitro* and *in vivo*. These results showed the versatility of this approach for general non-invasive force measurements *in vivo*.

Introduction

One of the technical hurdles in mechanobiology, a growing field of science at the interface of biology and physics, has been the methods to measure force in living cells non-invasively. The force or stress on the outer surface of the cells, or the plasma membrane, can be measured by the traction force microscopy (Polacheck & Chen, 2016). Fluorescent protein-based biosensors for force or tension at the cellular levels are also actively developed using Förster resonance energy transfer (Guo, Wang, Sachs, & Meng, 2014; Meng & Sachs, 2012; Meng, Suchyna, & Sachs, 2008). Optical tweezers have been used to measure force exerted on the lipid droplets in cultured cells or in Drosophila embryos (Jun, Tripathy, Narayanareddy, Mattson-Hoss, & Gross, 2014; Mas, Farre, Sancho-Parramon, Martin-Badosa, & Montes-Usategui, 2014; Shubeita et al., 2008), but its application to other organelles or subcellular structures is difficult. The Stokes relation can be theoretically used to estimate the drag force on the organelles moving at the velocity v as $F=6\pi\eta r v$. But, the viscosity η and the diameter of the organelle r need to be measured, the latter of which is often difficult for small organelles whose size is close to or below the diffraction limit of the microscope resolution. One may think that a friction coefficient $\Gamma=6\pi\eta r$ can be estimated from the diffusion coefficient of an organelle, D via the Einstein relation $D=k_{\mathrm{B}}T/\Gamma$, which is a one kind of the fluctuation-dissipation theorem (FDT) valid in near equilibrium. However, FDT is reported to be violated in various living cellular systems (Dinis, Martin, Barral, Prost, & Joanny, 2012; K. Hayashi et al., 2013; Turlier et al., 2016). We have previously reported that the Einstein relation is violated for organelle transports which was regarded as a complex non-equilibrium phenomena far from equilibrium (K. Hayashi et al., 2013). Therefore, force measurement in living cells needs essentially new physics beyond equilibrium statistical mechanics and the linear response theories.

A good example that needs force measurements is the axonal transport of vesicles. They are transported mainly by kinesins from the cell body to the periphery (anterograde) and dynein for the reverse direction (retrograde) (Hirokawa, Noda, Tanaka, & Niwa, 2009). Although many studies to date have elucidated their biological or functional importance, many physical or biophysical properties are still unclear (Encalada & Goldstein, 2014). For example, there is still controversy regarding the relationship between motor number, velocity and force. The *in vitro* velocity of purified kinesin-1 is around 1 μm/s and does not change with increasing motor

number, while the cargo velocity in the axon is often much faster, close to 5 μm/s (Allen, Metuzals, Tasaki, Brady, & Gilbert, 1982; Chiba et al., 2014) and apparently is dependent on the motor number (Reis et al., 2012). Mammalian dynein is more controversial. Many studies report its maximum force as only around 1 pN (A. G. Hendricks, Holzbaur, & Goldman, 2012; Mallik, Carter, Lex, King, & Gross, 2004; Rai, Rai, Ramaiya, Jha, & Mallik, 2013), though a few studies report values close to that of kinesin (Belyy et al., 2016; Nicholas et al., 2015; Toba, Watanabe, Yamaguchi-Okimoto, Toyoshima, & Higuchi, 2006).

To investigate these questions, here we propose a non-invasive force measurement by using the fluctuation theorem (FT). FT is a new universal law for entropy production in small non-equilibrium systems actively studied in the field of physics, and is considered as a generalized form of FDT, which connects energy dissipation to fluctuation (Ciliberto, Joubaud, & Petrosyan, 2010). In previous studies, for example, we have established that the FT can be applied to estimate molecular energies from the fluctuation property of bio-molecules *in vitro* (Kumiko Hayashi, Ueno, Iino, & Noji, 2010). This approach enables the estimation of the energy or force from only the passive measurement, the fluctuation of the movement. Thus, it is a fully passive and non-invasive method, potentially suitable for measurements in the living cells.

Results

Overview of the Theory

The quantity to be discussed in this study is force (F) generated by motors hauling a single cargo. In the stationary state, it is balanced by the drag force. The major cause of energy dissipation during the transport is the drag force, which would be increased with friction due to collisions or interactions with various cytoplasmic components such as water molecules, macro molecules, other organelles or cytoskeletal elements. Because the increase of friction slows diffusion, there should be an inverse relation between the drag force and the fluctuation (Figure 1), which is formulated by the FT as follows (see supplementary text for theoretical details):

$$\frac{F}{k_{\mathrm{B}}T_{\mathrm{eff}}} = \ln\left[P(\Delta X)/P(-\Delta X)\right]/\Delta X \qquad (1)$$

where ΔX is the displacement of the cargo calculated from the center position of a cargo as $\Delta X = X(t+\Delta t) - X(t)$, $P(\Delta X)$ is the probability distribution of ΔX, k_{B} is the Boltzmann constant. T_{eff}

is the effective temperature, which is a generalized measure of temperature in a non-equilibrium system (Cugliandolo, 2011; Dieterich, Camunas-Soler, Ribezzi-Crivellari, Seifert, & Ritort, 2015; Kumiko Hayashi & Sasa, 2004; Mizuno, Tardin, Schmidt, & MacKintosh, 2007).

Validation of FT with kinesin-driven beads *in vitro*

Before applying this theory to a real biological target, we first experimentally characterized the empirical parameter, effective temperature T_{eff}, by analyzing the bead-movement along a microtubule conveyed by a single or two kinesin molecules *in vitro*. The beads were prepared in a condition that most of the beads showed processive runs with stall forces at around 8 pN or 16 pN (Figure 2–figure supplements 1), indicating that each run was conveyed by one or two kinesin molecules (dimers) (Furuta et al., 2013). The net force F exerted on the bead was controlled by optical tweezers as $F=F_{\mathrm{m}}-F_{\mathrm{opt}}\,(=\Gamma v)$ where F_{m} and F_{opt} are the forces produced by the kinesin motors and the load by the optical tweezers, respectively.

The fluctuation of the bead displacement was analyzed as follows. The traces of bead movement were divided into several segments so that the bead velocity, which is proportional to the drag force, could be regarded to be constant in each segment (Figure 2A). The displacement was calculated in each segment with a fixed time interval Δt as $\Delta X=X(t+\Delta t)-X(t)$ (Figure 2B). The probability distribution of $P(\Delta X)$ was fitted with a Gaussian function (Figure 2C) to calculate the right-hand term of equation (1)

$$\chi=\ln\left[P(\Delta X)/P(-\Delta X)\right]/\Delta X \qquad (2)$$

As expected theoretically, χ showed dependence on the time interval of the analysis Δt with convergence at $\Delta t\geq 20$ ms (Figure 2D) (see supplementary text for detail). The value of χ at $\Delta t=30$ ms was used as the converged value χ^*. This is because equation (1) is a macroscopic relation valid for the time scales of the fluctuation that dominate the drag force. Thus, equation (1) should be rewritten as

$$F=k_{\mathrm{B}}T_{\mathrm{eff}}\chi^* \qquad (1')$$

which we tested by plotting the converged value χ^*, against F (Figure 2E). Here, the force F was measured independently by using Stokes law $F=\Gamma v$. The friction coefficient Γ was determined as 2.9 ± 0.4 μN s/m (mean ± SEM, n=4) from the power spectrum density of the same bead at the trap center of the optical tweezers before the run (Bormuth, Varga, Howard, & Schäffer, 2009)

(Figure 2–figure supplement 1 B, C). This value is consistent with the previous reports (Bormuth et al., 2009; Okada & Hirokawa, 1999; Mark J. Schnitzer & Block, 1997). Here, the Gaussian distribution of ΔX gives the estimate for the diffusion coefficient D as 0.003 $\mu m^2/s$. This value is twice larger than expected from the Einstein relation $D=k_BT/\Gamma$ with the parameter values for Γ =2.9 μN s/m and T=300 K, which shows the violation of this relation only valid for the equilibrium systems, and experimentally supports the necessity to extend FDT by introducing the effective temperature as in equations (1) and (1').

As shown in Figure 2E, the data points aligned linearly, as expected from equation (1'). The slope of the plot F/χ^* gives the effective temperature as k_BT_{eff}. Here, it should be noted that the data points include both beads driven by a single kinesin molecule (closed square, stall force <12 pN) and by two kinesin molecules (open square, stall force >12 pN). Still the values for the effective temperature were scattered around T_{eff}=650K, indicating that the effective temperature was insensitive to the number of the active motors on the bead, velocity or force.

Fluctuation measurement of axonally transported vesicles *in vivo*

Next, we examined the validity of FT with a real biological system, the axonal transport of endosomes in supracervical ganglion (SCG) neurons. The endosomes were selectively stained with a membrane-staining dye, DiI (Figure 3A). As established previously, most endosomes show linear movement along the axon anterogradely (to the axon terminal) or retrogradely (to the cell body). Although they sometimes show stochastic switching of the velocity or reversal of the direction, the fluctuation analyzed here is the fluctuation of the displacement around a constant velocity. Thus, the segment of unidirectional movement of constant velocity was chosen for the analysis (boxed regions in Figure 3B).

The movement of the endosome was recorded at the frame rate of 98 frames per sec. The position of the endosome was determined as the centroid of the fluorescent spot with the accuracy of 8 nm (see Methods for details). The degree of fluctuation χ (equation (2)) was calculated from the Gaussian distribution $P(\Delta X)$ (Figure 3C) of the displacement during the time interval Δt, namely $\Delta X(t)= \Delta X(t+\Delta t)- \Delta X(t)$ as described above (see Methods for details, and Figure 3–figure supplement 1 for the evaluations of the errors). Here we note that the assumption

of white Gaussian noise in $X(t)$ (supplementary text) was checked by the Gaussian forms of $P(\Delta X)$ (Figure 3C) and the power spectrum density $S(\nu)$ of the position $X(t)$ (Figure 3D).

The degree of fluctuation χ thus calculated showed convergence (χ^*) but with a relaxation time two times longer than that of the *in vitro* kinesin-coated beads (Figure 2D, 3E, 3–figure supplement 2A). The relaxation time did show dependency on the enzymatic turnover rate (Figure 3–figure supplement 2B, C), but the relaxation time was much longer than the enzymatic cycle time (~10 ms/molecule with saturating ATP for kinesin). The microenvironment around the vesicle, especially its viscoelastic nature, would affect the relaxation time as well.

Validation of FT with axonally transported vesicles *in vivo*

To validate FT (equation (1')), we first searched for the traces that contain two successive constant velocity segments (~2 s duration for each segment) with different velocities as shown in Figure 3B, because such traces would enable us to test FT without further estimation of the parameter values.

For each vesicle, its size or surrounding environment will not change substantially during the few seconds of the run event. Then, the friction efficient Γ would be same for both before and after the velocity change. The drag forces in the two velocity segments are written as $F_1=\Gamma v_1$ and $F_2=\Gamma v_2$, respectively, given by the Stokes law. If FT (equation (1')) holds with the same T_{eff} value for both segments, $F_1=k_{\mathrm{B}}T_{\mathrm{eff}}\,\chi_1^*$ and $F_2=k_{\mathrm{B}}T_{\mathrm{eff}}\,\chi_2^*$. Their ratio thus gives unity,

$$\frac{v_1 / v_2}{\chi_1^* / \chi_2^*} = 1 \qquad (3)$$

The results (Figure 4A) were consistent with this relation, suggesting that the effective temperature would take same or similar value for each vesicle during the few seconds of the run event.

As the second validation, we tried to examine the relationship between the drag force and the fluctuation among different vesicles. The measurement of the drag force is generally difficult because the friction coefficient Γ is difficult to estimate for the moving vesicles. However, Γ can be estimated for a tethered vesicle from the power spectrum of its Brownian movement. We,

therefore, searched for the trajectories (14 from > 200 traces) with a constant velocity long run (~ 2 s in duration) followed by a long pause (no net movement > 3 s) (Figure 4–figure supplement 1A). The latter, pause segment, was used to estimate the friction coefficient Γ (Figure 4–figure supplement 1B, C). This value was applied to the former, running segment, because the friction coefficient, which is determined by the size of the endosome and its environment, will not change much during the single run event. The drag force was thus calculated from the Stokes law: $F=\Gamma v$. As shown in Figure 4B-D, there were no clear relationship between the velocity and the fluctuation χ^* (Figure 4B), but the drag force was proportional to the fluctuation χ^* (Figure 4C). This is because the friction coefficient varies among vesicles. The plot in Figure 4D shows that Γ is roughly proportional to the vesicle size, though the proportional constant or the effective viscosity was ~1000 times larger than water as reported previously in non-neuronal cells (Wirtz, 2009). It should also be noted here that the Einstein relation $D= k_BT/\Gamma$ is violated. The diffusion coefficient D was estimated as ~0.01 $\mu m^2/s$ from the Gaussian distribution of ΔX, and this value was more than 10 times larger than expected from the Einstein relation with the values for Γ =~10 μN s/m and T=300 K. The extent of the violation was larger for the *in vivo* organelle transport than for the *in vitro* bead movement discussed in the previous section, which would reflect the complex interactions in the *in vivo* environment.

More importantly, the proportional relation between the drag force and the fluctuation χ^* in Figure 4C implies that FT holds for these different vesicles in different neurons (n=14) with the same or similar value of proportional coefficient, or the effective temperature. There were no statistically significant differences between the effective temperature values between the anterograde and retrograde endosomes. These results would imply that the effective temperature would reflect the cellular environments surrounding the endosome rather than the number or other properties (e.g. kinesin or dynein) of the motor protein that conveys the vesicle.

The slope of the best fit line gives the estimate of this global effective temperature as T_{eff}=4200 K. This does not literally mean that the temperature of the cytoplasm is 4200 K. Although the exact physical meaning of the effective temperature is still controversial (Kumiko Hayashi & Sasa, 2004), it is often observed $T_{eff} > T$ in non-equilibrium systems (Cugliandolo, 2011). The most plausible interpretation would be that the fluctuation process(es) that dominantly determine

the drag force are actively driven by using energy 14 times higher than the thermal energy, which might reflect the recently reported active stirring of the cytoplasm by motor proteins (Fakhri et al., 2014). Here, the free energy obtained by single ATP hydrolysis is about 20 k_BT, which would give a reference for the energy scale of active processes in living cells.

Drag force measurement using FT for anterogradely transported endosomes in axon

Using the value of T_{eff}=4200 K calibrated for endosomes (n=14) described above, we analyzed the remaining traces for the anterogradely transported endosomes with the segments of constant velocity that lasted for longer than 3 seconds. The measure of the fluctuation χ was then calculated for the constant velocity region for each endosome for various intervals Δt from 10 ms to 100 ms, which confirmed that the time constant for the convergence was around Δt=50 ms (Figure 3E, 5A). We, therefore, analyzed the remaining shorter traces which had segments of constant velocity that lasted for about 2 seconds, with the interval Δt up to 50 ms.

As summarized in Figure 5A, B, the plots (79 runs) appeared to be clustered into several groups. The histogram of the χ values at Δt=50 ms, the proxy for the convergent value χ^*, showed discrete distribution, which was statistically confirmed by the *k*-means clustering (Method). Because χ^* is approximately proportional to force F (equation (1')), this discrete distribution of χ^* is most likely to reflect the force producing unit (FPU) in this system. At the same time, it also implies that the proportionality constant between the force and the fluctuation, or the effective temperature, does not vary much among these 79 vesicles from 76 neurons. Otherwise, the discrete force distribution by the presence of FPU would be obscured by the distribution of the effective temperatures.

By applying the global effective temperature value of 4200K (Figure 4C), the peak positions of the force distribution were multiples of about 5 pN. This value agrees well with the reported value for the force production by a single kinesin *in vitro* (M J Schnitzer, Visscher, & Block, 2000), suggesting that a single kinesin molecule would correspond to a single FPU in the anterogradely transported endosomes. There was a weak tendency toward more FPUs on larger endosomes (Figure 5B). The number of FPUs would thus not be tightly regulated to compensate

for the greater drag resistance for the larger vesicles, but would simply reflect the geometric constraints that larger vesicles have more space to accommodate additional FPUs.

It should be noted here that the velocity distribution does not show clear peaks (Figure 5–figure supplement 1). If the friction coefficient Γ were constant among different vesicles, the velocity would also distribute discretely as reported with frog melanosomes (Levi, Serpinskaya, Gratton, & Gelfand, 2006), because the velocity should be proportional to the drag force as $v=F/\Gamma$. For the endosomes in neurons, however, the discrete distribution of force was obscured because Γ varied much among different vesicles reflecting the large variance of the vesicle size (Figure 4D).

Force-velocity relations for anterogradely transported endosomes in axon

Assuming that no external forces are exerted on the endosomes transported in the axon, the drag force should be balanced with the force produced by the motor protein, most likely kinesin (Figure 1). Thus, the measured values for the force and the velocity should scatter along the force-velocity relation curve for the kinesin motor property.

For the anterogradely transported endosomes, one kinesin dimer molecule would most likely correspond to the anterograde FPU, because the previous biochemical measurement reported that only 1-4 kinesin dimers are bound to vesicles (Adam G Hendricks et al., 2010). Based on this assumption, we have compared the mechanical properties of kinesin *in vitro* and the force-velocity relation of the anterogradely transported endosome. The force-velocity relations were plotted (Figure 5C) along with the phenomenological model that describes the *in vitro* results of kinesin (M J Schnitzer et al., 2000). The force ranges for 1, 2, 3 and 4 kinesin molecules were consistent with the *in vivo* results, but the velocity was much faster *in vivo*. Better fitting was achieved by increasing the enzymatic turnover rate (Figure 5D), which might suggest the acceleration of the enzymatic reaction by the macromolecular crowding in the cytoplasm (Ellis, 2001).

Measurement and analysis of the force for retrogradely transported endosomes in axon

The traces for the retrogradely transported endosomes were similarly analyzed. Traces with the segments of constant velocity that lasted for longer than 3 seconds were first examined to confirm the time constant for the convergence as ~ 50 ms, and then analyzed the remaining shorter traces which had segments of constant velocity that lasted for about 2 seconds (Figure 6A). The plots (119 runs) were also clustered into several groups. The discrete distribution of the χ values at Δt=50 ms (the proxy for the convergent value χ^*) was statistically confirmed by the *k*-means clustering. Thus, the presence of FPU was also demonstrated with retrogradely transported endosomes. The number of FPUs showed a weak positive correlation to the endosome size (Figure 6B) as observed with the anterogradely transported endosomes (Figure 5B), which is consistent with the geometric constraints model (Figure 5B, inset) for the regulation of the number of FPUs on the endosome. Note that the discrete distribution of χ^* also gives another experimental support that the effective temperature does not vary much among these 119 vesicles from 112 neurons.

By applying the global effective temperature value of 4200K (Figure 4C), the peak positions of the force distribution were multiples of about 6 pN, similar to those with the anterogradely transported endosomes.

Although the force-velocity relations for dynein are still controversial, the phenomenological model (M J Schnitzer et al., 2000) for kinesin used in Figure 5C is a general phenomenological model which can be applied to a wide range of processive motor proteins including dynein by adjusting the parameters. We have, therefore, fitted the force-velocity relations of the retrograde vesicles (Figure 6C) to the same model. The maximum velocity was increased similarly with kinesin.

The maximum force of the best fit curve was around 10 pN and inconsistent with most *in vitro* studies that report only 1 pN for a single dynein molecule (A. G. Hendricks et al., 2012; Mallik et al., 2004; Rai et al., 2013). Several groups independently reported that dynein can be activated to produce maximum force around 5 pN (Belyy et al., 2016; Nicholas et al., 2015; Toba et al., 2006), and there might be a mechanism to increase the maximum force of dynein to 10 pN in the cytoplasm. Considering that the average number of dynein molecules on a single vesicle (Adam

G Hendricks et al., 2010) is two times larger than the average number of retrograde FPUs in this study, two dimers of dynein along with dynactin or other regulatory protein(s) might serve as a single FPU, as was recently reported for the cooperative, collective force production by multiple dynein molecules (Torisawa et al., 2014). Alternatively, only half of the dynein molecules on the endosome are activated to produce force up to 10 pN. Thus, the results obtained with this measurement suggested that our understanding is still limited on retrograde transport mechanism supported by dynein.

Discussion

In this study, we have demonstrated that FT is practically useful for the non-invasive force measurement *in vivo*. Theoretically, the proportionality constant between the entropy production and the fluctuation, or the effective temperature, is affected by many complex interactions in real biological systems and is not necessarily equal to the real temperature of the system (Cugliandolo, 2011; Zimmermann & Seifert, 2012). It is not clear a priori whether it takes same or similar values even in a single cell. However, as we have shown experimentally, the variance of the effective temperature T_{eff} (10% CV) was much smaller than that of the friction coefficient Γ (100% CV) for the axonally transported endosomes (Figure 4B, C). Hence, the number of the FPUs on the vesicle was reflected only to the fluctuation χ^* as a discrete distribution with distinct peaks (Figure 5A, B), but not to the velocity v (Figure 5–figure supplement 1). The large variance of Γ reflects the various sizes of the axonal endosomes (Figure 4D), and there was a weak positive correlation between the number of the FPUs and the endosome size (Figure 5B, 6B).

Although the physical or mechanistic details behind the small variance of T_{eff} remains unclear, it implies that calibration for T_{eff} is not necessary for each vesicle or neuron, but a single result of calibration can be applied to other vesicles. In this study, a single value of T_{eff} (4200K) can be applied to the ~200 vesicles analyzed here. The force value ~10 pN, thus determined, is consistent with previous *in vivo* measurements in macrophages (A. G. Hendricks et al., 2012). This force value, along with the other parameter values (the diameter of endosome $2r$ =500 nm, and the velocity v=2 μm/s) gives the effective viscosity η_{eff} as ~1000 cP by using the relation

$F=6\pi\eta_{\mathrm{eff}} r v$. This estimate is 1000x higher than water, but is consistent with the microrheology measurement in the cytoplasm with traces of similar sizes to the endosomes (Wirtz, 2009).

The maximum force or the stall force *in vivo* estimated from the force-velocity relation was also consistent with the results with purified or recombinant kinesin measured *in vitro* (M J Schnitzer et al., 2000). However, the force velocity relation *in vivo* showed large discrepancy from the *in vitro* one, not in the force but in the velocity (Figure 5C). Here, the velocity was directly measured from the trajectory. Therefore, the discrepancy is not likely to be caused by any potential ambiguities in the force estimation by FT. Since 4-fold increase in the velocity gives better fitting of the *in vitro* relations to the *in vivo* results (Figure 5D), most naïve interpretation of the results would be that kinesin will move 4 times faster *in vivo*. However, the *in vivo* velocity of constitutively active truncated kinesin-1 dimer does not differ much from the *in vitro* velocity. There might be some regulatory mechanisms to accelerate the velocity by the scaffold protein that anchors kinesin to the cargo vesicle as suggested from our previous analysis of the APP-transport vesicles (Chiba et al., 2014). Similarly, the force-velocity relation of the retrograde endosomes also suggested the presence of some cooperative, collective force production mechanisms for multiple dynein molecules *in vivo*. These issues were first realized by the drag force measurement *in vivo*, and are good examples to show the importance of the force measurements in the future studies.

In summary, we have established a FT-based method to estimate the drag force exerted on the vesicles transported in living cells by analyzing only their movement. Unlike other existing methods for force measurement, it is fully passive and non-invasive. We used vital staining with a fluorescent dye for a selective visualization of endosomes, but DIC or phase-contrast image of unstained samples can be used as well. Thus, this non-invasive method would serve as a powerful and versatile tool for basic research in the field of intracellular transport, as well as some potential applications for the examination of the molecular motor functions in clinical samples. Furthermore, the violation of FDT has been reported in various biological systems both *in vitro* and *in vivo* such as actomyosin (Mizuno et al., 2007), DNA hairpins (Dieterich et al., 2015) and red blood cells (Turlier et al., 2016). With the idea of effective temperature, as a violation factor of the fluctuation-dissipation theorem, other fluctuation theories of non-

equilibrium statistical mechanics other than the FT used in this paper, such as the Jarzynski equality (Jarzynski, 1997) and the Crooks fluctuation theorem (Crooks, 1999) may connect the non-equilibrium fluctuation to the energetic properties of systems. Thus, our method can be expanded to other mechanical processes in living cells, and would provide a basis for the versatile general method for the non-invasive *in vivo* mechanical measurements.

Materials and Methods

Reagents

All reagents were purchased from Wako or Sigma-Aldrich, unless otherwise stated.

Purification of kinesin for *in vitro* assay

As described previously (Okada & Hirokawa, 1999), a constitutive active dimer construct of mouse kinesin-1 (KIF5C 1-560aa) was subcloned into a plasmid vector pET21B (EMD biosciences). An *in vivo* biotinylation tag, BCCP (biotin carbonyl carrier protein, Promega) was inserted to the C-terminus of the construct. The plasmid was introduced into bacterial cell BL21(DE3)RIL (Agilent). The transformant was cultured with 2x YT medium supplemented with 30 mM phosphate buffer (pH 7.4) at 37 °C to mid-log phase (OD600=1.0). The culture was cooled down to 23 °C, and the protein expression was induced by adding 0.1 mM (final concentration) isopropyl β–D-1-thiogalactopyranoside (IPTG). The bacterial cells were collected 5 hrs after induction, and rinsed with ice-cold phosphate-buffered saline (PBS) supplemented with phenylmethyl-sulfonyl fluoride (PMSF).

Then, the bacterial cells were resuspended with five volumes of buffer A (HEPES 50 mM, potassium acetate 500 mM, magnesium acetate 5 mM, imidazole 10 mM, pH 7.4 adjusted with KOH) supplemented with ATP 0.1 mM and the following protease inhibitors: Pefabloc SC 1 mM, Leupeptin 20 μM, Pepstatin A 10 μM, Nα-p-tosyl-L-arginine methyl ester (TAME) 1 mM. The bacterial cell wall was solubilized with lysozyme (2 mg/ml). DNase I (10 μg/ml) was added to reduce viscosity by the bacterial genomic DNA. Then bacterial cells were broken by sonication.

The soluble protein was recovered by centrifugation at 20,000 xg for 30 min, and was applied to the immobilized metal affinity chromatography column TALON (Takara). The protein was eluted with buffer B (PIPES 20 mM, imidazole 250 mM, magnesium sulfate 2 mM, EGTA 1 mM) supplemented with ATP 0.1 mM and protease inhibitors. The peak fractions were pooled and stored at -80°C after snap-freezing in liquid nitrogen.

Preparation of microtubules

Tubulin was purified by the high-molarity PIPES buffer method (Castoldi & Popov, 2003) with modifications (Yajima et al., 2012). Porcine brains were cleaned by removing meninges, blood clots and vessels in washing buffer (PIPES 50 mM, PMSF 5 mM, pH 6.8). They were homogenized in a pre-chilled Waring blender with PEM buffer (PIPES 100 mM, EGTA 1 mM, $MgCl_2$ 1 mM, pH 6.8 adjusted with KOH) supplemented with PMSF 0.5 mM, Leupeptin 2 µM and DTT 0.5 mM. After clarification with centrifugation at 15,200 xg, 60 min, microtubules were polymerized by warming the supernatant to 37 °C after supplementation with MgATP 1 mM, MgGTP 0.5 mM and glycerol. The polymerized microtubules were collected by ultracentrifugation at 100,000 xg 37 °C. Then, they were depolymerized in ice-cold P_{1000}EM buffer (PIPES 1,000 mM, EGTA 1 mM, $MgCl_2$ 1 mM, pH 6.8 adjusted with KOH) at 0 °C. The supernatant was collected by ultracentrifugation at 100,000 xg, 4 °C. The polymerization and depolymerization cycles were repeated four times, and the final supernatant was pooled and stored in liquid nitrogen.

TMR (tetramethyl rhodamine)-labeled microtubules were prepared as follows. Microtubules were polymerized in PEM buffer supplemented with 1 mM GTP at 37 °C. Then, 5-(and-6)-Carboxytetramethylrhodamine, Succinimidyl Ester (Life Technologies) was added at 5-10 molar excess. Labeled microtubules were separated from free dye by ultracentrifugation through glycerol cushion, and were resuspended with ice-cold PEM buffer. The microtubules were depolymerized by cooling down the solution to 0°C, and the supernatant was collected by ultracentrifugation at 100,000 xg, 4 °C. The labeling efficiency was measured spectroscopically, and stored in liquid nitrogen.

Bead assay

For the bead assay, the carboxy-modified fluorescent 0.5 µm latex bead (Life Technologies) was biotinylated with (+)-biotinyl-3,6,9,-trioxaundecanediamine (Amine-PEG3-biotin, Pierce) using condensation agent DMT-MM(4-(4,6-dimethoxy-1,3,5-triazin-2-yl)-4-methyl-morpholinium). The purified recombinant kinesin dimer was immobilized on the bead surface via streptavidin (Sigma) in assay buffer (PIPES 80 mM, magnesium acetate 5 mM, EGTA 1 mM, ATP 2 mM, casein 0.5 mg/ml, taxol 10 µM, β-mercaptoethanol 10 mM, catalase 0.1 mg/ml, glucose 10 mM, glucose oxidase 0.05 mg/ml, pH 6.8). Diluted, TMR-labeled microtubules were absorbed to the

glass surface of the flow cell chamber, and the remaining surface was coated with a biocompatible polymer Lipidure-BL-103 (NOF). Then, the kinesin-coated beads were injected into the chamber. The optical tweezers instrument is based on the inverted microscope IX2 (Olympus). The beam of near infra-red laser (1064 nm BL-106C, Spectra-Physics) was collimated to fill the back aperture of the objective lens (PlanApo 60x/1.40, Olympus). The bead trapped at the focus was illuminated with green laser (532 nm, 400 mW, Genesis CX, Coherent), and its image was projected to EMCCD camera iXon DU-860D-CS0-#BV (Andor). The images were recorded at the speed of 400 frames per second at 22 °C. The constant velocity segments (n=45) used in the analysis (Figure 2E) were cut from 31 runs from 5 different bead assays.

Primary culture of neurons

Superior cervical ganglions (SCGs) isolated from 3 weeks old ICR mice (male) were enzymatically treated in 0.5 % trypsin (Sigma) followed by 2 hr treatment with 0.5 % collagenase (Worthington). Dissociated cells were rinsed with DMEM/F12 containing 10 % heat inactivated bovine serum (Life Technologies), and plated onto Matrigel (BD-Biosciences)-coated glass-bottom dish (Matsunami). The neurons were cultured for two to four days with a DMEM/F12 medium supplemented with 10 % heat inactivated bovine serum and 200 ng/ml 2.5S nerve growth factor. All the animal experiments were conducted in compliance with the protocol which was approved by Institutional Animal Care and Use Committee, Tohoku University.

Observation of endosomes and image analysis

The neurons were stained for 10 min with 100 nM DiI (Life Technologies), and then observed with a fluorescent microscope (IX71, Olympus) equipped with a heating plate (CU-201, Live Cell Instrument). The images of the motile endosomes were obtained with a 100x objective lens (UPlanFL 100x/1.3, Olympus) and an EMCCD camera LucaS (Andor) at 98 frames per second at 37 °C. The center position of each endosome was determined from the recorded image using ImageJ (Rasband, 1997), and the displacement from the position in the first frame was calculated for each frame. Here we focused on the displacement along the direction of the motion $X(t)$. The data were collected from 34 preparations (culture dishes). 79 endosomes from 76 different cells for anterograde, and 119 endosomes from 112 different cells for retrograde were investigated. The cells for observation were chosen randomly after visual inspection, and the trajectories with

longer than 2 second constant velocity run(s) were selected for the analyses. The constant velocity segment was selected by fitting the trajectory with a constant velocity movement, so that the residual does not exceed the variance perpendicular to the movement. The accuracy of the position measurement was verified with fluorescent beads with a similar size and fluorescent intensity to the endosomes (300 nm latex bead, Polyscience). The standard deviation of the position of the bead tightly attached to the glass surface was 8.4±0.4 nm (5 different beads in 2 independent preparations), which is much smaller than the displacement between frames ΔX ($=X(t+\Delta t)-X(t)$) analyzed in this study and would affect the accuracy of the fluctuation measurement by less than 10% CV, within the range of the estimation errors in the fluctuation (Figure 3–figure supplement 1).

Preparation of permeabilized and reactivated neuron

For some experiments, the plasma membrane of the neuron was permeabilized to control the cytoplasmic ATP concentration (Okada, Sato-Yoshitake, & Hirokawa, 1995). Clarified brain homogenate was used to compensate for the loss of cytoplasmic components after membrane permeabilization. Mouse brain was cleaned in ice-cold PBS and homogenized with three volumes of KHMgE buffer (K-acetate 115 mM, Hepes 20 mM, MgCl2 1 mM, EGTA 1 mM, pH 7.4) supplemented with protease inhibitor cocktail (Complete EDTA-free, Roche). The homogenate was clarified by the successive centrifugation at 1,000 xg 10min and 100,000 xg 1 hr. The brain cytosol thus prepared was aliquoted and snap frozen with liquid nitrogen. The assay buffer was prepared just before use by mixing the brain cytosol with equal volume of KHMgE buffer supplemented with ATP regeneration system (0.125 mM or 0.0125 mM ATP, 10 mM creatine phosphate, 8 U/ml creatine phosphokinase), protease inhibitor cocktail (Complete EDTA-free) and 5 mM beta-mercapto ethanol. The neurons were first rinsed with KHMgE, then followed by 8 min incubation with the assay buffer containing 0.01 mg/ml digitonin. Fluorescent dextran (VECTOR) was used to examine the membrane permeabilization after digitonin treatment. The data were collected from 11 preparations (culture dishes) for [ATP]=125 μM (62 endosomes from 53 cells) and 6 preparations (culture dishes) for [ATP]=12.5 μM (30 endosomes from 23 cells).

Measurement of the friction coefficient from the power spectrum

The power spectrum density, $S(\nu)$, of the bead position attached but not moving along the microtubule is known to be proportional to the Lorentzian function $1/(1+(\Gamma/\kappa_{\mathrm{eff}}\ \nu)^2)$ where ν is frequency and κeff is an effective stiffness (Bormuth et al., 2009). Here, κeff can be estimated from the equilibrium probability distribution of the bead position: $P_B(X)$ $(=(2\pi\ k_BT/\kappa_{\mathrm{eff}})^{0.5}\exp(-\kappa_{\mathrm{eff}}X^2/2k_BT))$. The same relations can be applied to the pausing motion of the endosomes. Therefore, we first examined the distribution of $X(t)$ and fitted with a Gaussian distribution to estimate κeff. Then, the power spectrum density of $X(t)$ was calculated as

$$S(\nu) = \frac{\langle |X_\nu|^2 \rangle}{\tau_s} \tag{M1}$$

$$X_\nu = \int_{-\tau_s/2}^{\tau_s/2} X(t) e^{i2\pi\nu t} dt \tag{M2}$$

where ν is a frequency and $\tau_s=N_W/98$ s. Note that the recording rate was 98 fps, N_w is the window size, and $\langle\cdot\rangle$ denotes the time average over the trajectory investigated. The Lorentzian function was fitted to this spectrum to estimate Γ. The estimated values of Γ had error of approximately 20% (Figure 2–figure supplement 1C, Figure 4–figure supplement 1C).

Analysis of fluctuation using FT

The value of χ is defined as

$$\chi = \ln[P(\Delta X) / P(-\Delta X)] / \Delta X \tag{M3}$$

from the distribution, $P(\Delta X)$, of the displacement $\Delta X = X(t+\Delta t)-X(t)$. Since the noise was confirmed to be Gaussian (Figure 3C, D), $P(\Delta X)$ was fitted with a Gaussian function

$$P(\Delta X) = \exp\left(-\left(\Delta X - b\right)^2 / 2a\right) / (2\pi a)^{0.5} \tag{M4}$$

where the fitting parameters a and b correspond to the variance and the mean of the distribution. By substituting equation (M4) to equation (M3),

$$\chi = 2b / a \tag{M5}$$

Thus, χ was calculated as $2b/a$ for each $P(\Delta X)$ for various interval Δt from 10 ms to 100 ms. The values for a and b were also estimated from the cumulative Gaussian distribution of ΔX, and directly as the sample variance ($a=\langle(\Delta X-\langle\Delta X\rangle)^2\rangle$) and the average ($b=\langle\Delta X\rangle$). These two estimations provided the same values of a and b within the error of χ (Figure 3–figure

supplement 1). The converged value χ^* was determined by plotting χ against Δt as shown in Figure 2D and 3E ($\chi^* = \chi$ at 30 ms in Figure 2, and $\chi^* = \chi$ at 51 ms in Figure 4-6.)

T_{eff} was estimated from the trajectories of endosomes that paused just before or after the run (Figure 4–figure supplement 1). For these trajectories (n=14), the drag coefficient Γ was estimated from the power spectrum during the pause period as described in the previous section, and the fluctuation χ^* was determined from the constant velocity segment. Then, T_{eff} was estimated from the following relation:

$$k_{\mathrm{B}}T_{\mathrm{eff}} = \frac{F}{\chi^*} = \frac{\Gamma v}{\chi^*} \qquad \text{(M6)}$$

as shown in Figure 4C. The T_{eff} value (=4200K) thus determined was used for all other endosomes analyzed in this paper.

k-means clustering

The χ-Δt plots for the anterograde and retrograde endosomes (Figure 5A, 6A) were classified statistically by using a *k*-means clustering method using a program package R with a library "cluster". First, the number of clusters *k* was determined by calculating AIC (Akaike's Information Criterion) for χ-Δt plots. In the case of the anterograde χ-Δt plots (Figure 5A), AIC values were -122.1 for k=2, -134.6 for k=3, -140.2 for k=4, and -134.4 for k=5. In the case of the retrograde χ-Δt plots (Figure 6A), AIC values were -232.3 for k=2, -246.6 for k=3, -247.0 for k=4 and -245.3 for k=5. From these AIC values along with the Gap statistics, the most probable values of k were determined as k =4 for anterograde and k=3 for retrograde, respectively. The initial value for the k-th cluster center trajectory χ_c^k was chosen as the k-th peak value of χ^* (the arrows in Figure 5A, 6A). Each trajectory of χ was classified to the cluster based on the mean square deviation from χ_c^k. Then χ_c^k was renewed as the mean of the trajectories classified to that cluster. This procedure was repeated until convergence.

Analysis of the force-velocity relation

We adopted the widely-accepted model of kinesin-1 (M J Schnitzer et al., 2000) for the analysis of the measured force-velocity relations. In this model, velocity is expressed as the function of ATP concentration as

$$v = \frac{d}{\frac{1}{k_{cat}} + \frac{1}{k_b[ATP]}} \tag{M7}$$

where d is the step size (=8 nm). k_{cat} and k_b are the catalytic turnover rate and the apparent second order rate constant for ATP binding (=ratio of kcat and Michaelis-Menten constant K_M). The load (F) dependencies are introduced as

$$k_{cat} = \frac{k_{cat}^0}{1 - q_{cat}\left(1 - \exp\left(\frac{F\delta}{k_B T}\right)\right)} \tag{M8}$$

$$k_b = \frac{k_b^0}{1 - q_b\left(1 - \exp\left(\frac{F\delta}{k_B T}\right)\right)} \tag{M9}$$

The values for the parameters k_{cat} and k_b were taken from the reported *in vitro* results (M J Schnitzer et al., 2000): q_{cat}=0.0062, q_b=0.04.

The ATP concentration in the cytoplasm is around 4 mM. Since it is much higher than K_M which is around 50 μM for both kinesin and dynein, the inaccuracy in the ATP concentration does not affect the results. k_{cat}^0 was determined from the maximum velocity of endosome observed in our experiments (3.9 μm/s and 4.1 μm/s for anterograde and retrograde runs, respectively). Namely, $k_{cat}^0 = v_{max}/d$ (488 /s and 515 /s for anterograde and retrograde runs, respectively). For the analysis of anterograde runs, the characteristic distance δ was set to 3.8 nm, which is the value reported with kinesin-1 (M J Schnitzer et al., 2000). For the retrograde data sets, the value δ was estimated to be 3.6 nm by fitting the model.

References and Notes

Allen, R. D., Metuzals, J., Tasaki, I., Brady, S. T., & Gilbert, S. P. (1982). Fast axonal transport in squid giant axon. *Science (New York, N.Y.)*, *218*(4577), 1127–9. Retrieved from http://www.ncbi.nlm.nih.gov/pubmed/6183744

Belyy, V., Schlager, M. A., Foster, H., Reimer, A. E., Carter, A. P., & Yildiz, A. (2016). The mammalian dynein–dynactin complex is a strong opponent to kinesin in a tug-of-war competition. *Nature Cell Biology*, *18*(9), 1018–1024. https://doi.org/10.1038/ncb3393

Bormuth, V., Varga, V., Howard, J., & Schäffer, E. (2009). Protein friction limits diffusive and directed movements of kinesin motors on microtubules. *Science (New York, N.Y.)*, *325*(5942), 870–3. https://doi.org/10.1126/science.1174923

Castoldi, M., & Popov, A. V. (2003). Purification of brain tubulin through two cycles of polymerization-depolymerization in a high-molarity buffer. *Protein Expression and Purification*, *32*(1), 83–8. https://doi.org/10.1016/S1046-5928(03)00218-3

Chiba, K., Araseki, M., Nozawa, K., Furukori, K., Araki, Y., Matsushima, T., … Suzuki, T. (2014). Quantitative analysis of APP axonal transport in neurons: role of JIP1 in enhanced APP anterograde transport. *Molecular Biology of the Cell*, *25*(22), 3569–3580. https://doi.org/10.1091/mbc.E14-06-1111

Ciliberto, S., Joubaud, S., & Petrosyan, A. (2010). Fluctuations in out-of-equilibrium systems: from theory to experiment. *Journal of Statistical Mechanics: Theory and Experiment*, *2010*(12), P12003. https://doi.org/10.1088/1742-5468/2010/12/P12003

Crooks, G. E. (1999). Entropy production fluctuation theorem and the nonequilibrium work relation for free energy differences. *Physical Review E*, *60*(3), 2721–2726. https://doi.org/10.1103/PhysRevE.60.2721

Cugliandolo, L. F. (2011). The effective temperature. *Journal of Physics A: Mathematical and Theoretical*, *44*(48), 483001. https://doi.org/10.1088/1751-8113/44/48/483001

Dieterich, E., Camunas-Soler, J., Ribezzi-Crivellari, M., Seifert, U., & Ritort, F. (2015). Single-molecule measurement of the effective temperature in non-equilibrium steady states. *Nature Physics*, *11*(11), 971–977. https://doi.org/10.1038/nphys3435

Dinis, L., Martin, P., Barral, J., Prost, J., & Joanny, J. F. (2012). Fluctuation-Response Theorem for the Active Noisy Oscillator of the Hair-Cell Bundle. *Physical Review Letters*, *109*(16), 160602. https://doi.org/10.1103/PhysRevLett.109.160602

Ellis, R. J. J. (2001). Macromolecular crowding: obvious but underappreciated. *Trends in Biochemical Sciences*, *26*(10), 597–604. https://doi.org/10.1016/S0968-0004(01)01938-7

Encalada, S. E., & Goldstein, L. S. B. (2014). Biophysical Challenges to Axonal Transport: Motor-Cargo Deficiencies and Neurodegeneration. *Annual Review of Biophysics*, *43*(1), 141–169. https://doi.org/10.1146/annurev-biophys-051013-022746

Fakhri, N., Wessel, A. D., Willms, C., Pasquali, M., Klopfenstein, D. R., MacKintosh, F. C., & Schmidt, C. F. (2014). High-resolution mapping of intracellular fluctuations using carbon nanotubes. *Science*, *344*(6187). Retrieved from http://science.sciencemag.org/content/344/6187/1031.full

Furuta, K., Furuta, A., Toyoshima, Y. Y., Amino, M., Oiwa, K., & Kojima, H. (2013). Measuring collective transport by defined numbers of processive and nonprocessive kinesin motors. *Proceedings of the National Academy of Sciences*, *110*(2), 501–506. https://doi.org/10.1073/pnas.1201390110

Guo, J., Wang, Y., Sachs, F., & Meng, F. (2014). Actin stress in cell reprogramming. *Proceedings of the National Academy of Sciences of the United States of America*, *111*(49), E5252-61. https://doi.org/10.1073/pnas.1411683111

Hayashi, K., Pack, C. G. G., Sato, M. K. K., Mouri, K., Kaizu, K., Takahashi, K., & Okada, Y. (2013). Viscosity and drag force involved in organelle transport: investigation of the fluctuation dissipation theorem. *The European Physical Journal. E, Soft Matter*, *36*(12), 136. https://doi.org/10.1140/epje/i2013-13136-6

Hayashi, K., & Sasa, S. (2004). Effective temperature in nonequilibrium steady states of Langevin systems with a tilted periodic potential. *Physical Review E*, *69*(6), 66119. https://doi.org/10.1103/PhysRevE.69.066119

Hayashi, K., & Sasa, S. (2005). Decomposition of force fluctuations far from equilibrium. *Physical Review E*, *71*(2), 20102. https://doi.org/10.1103/PhysRevE.71.020102

Hayashi, K., Ueno, H., Iino, R., & Noji, H. (2010). Fluctuation Theorem Applied to F1-ATPase. *Physical Review Letters*, *104*(21), 218103. https://doi.org/10.1103/PhysRevLett.104.218103

Hendricks, A. G., Holzbaur, E. L. F., & Goldman, Y. E. (2012). Force measurements on cargoes in living cells reveal collective dynamics of microtubule motors. *Proceedings of the National Academy of Sciences*, *109*(45), 18447–18452. https://doi.org/10.1073/pnas.1215462109

Hendricks, A. G., Perlson, E., Ross, J. L., Schroeder, H. W., Tokito, M., & Holzbaur, E. L. F. (2010). Motor coordination via a tug-of-war mechanism drives bidirectional vesicle transport. *Current Biology : CB*, *20*(8), 697–702. https://doi.org/10.1016/j.cub.2010.02.058

Hirokawa, N., Noda, Y., Tanaka, Y., & Niwa, S. (2009). Kinesin superfamily motor proteins and intracellular transport. *Nature Reviews Molecular Cell Biology*, *10*(10), 682–696. https://doi.org/10.1038/nrm2774

Howard, J. (2001). Thermal Forces and Diffusion. In *Mechanics of Motor Proteins and the Cytoskeleton* (pp. 49–74). Sunderland, MA: Sinauer.

Jarzynski, C. (1997). Nonequilibrium Equality for Free Energy Differences. *Physical Review Letters*, *78*(14), 2690–2693. https://doi.org/10.1103/PhysRevLett.78.2690

Jun, Y., Tripathy, S. K., Narayanareddy, B. R. J., Mattson-Hoss, M. K., & Gross, S. P. (2014). Calibration of optical tweezers for in vivo force measurements: how do different approaches compare? *Biophysical Journal*, *107*(6), 1474–84. https://doi.org/10.1016/j.bpj.2014.07.033

Levi, V., Serpinskaya, A. S., Gratton, E., & Gelfand, V. (2006). Organelle transport along microtubules in Xenopus melanophores: evidence for cooperation between multiple motors. *Biophysical Journal*, *90*(1), 318–27. https://doi.org/10.1529/biophysj.105.067843

Mallik, R., Carter, B. C., Lex, S. A., King, S. J., & Gross, S. P. (2004). Cytoplasmic dynein functions as a gear in response to load. *Nature*, *427*(6975), 649–652. https://doi.org/10.1038/nature02293

Mas, J., Farre, A., Sancho-Parramon, J., Martin-Badosa, E., & Montes-Usategui, M. (2014). Force measurements with optical tweezers inside living cells. *Proceedings of SPIE - The International Society for Optical Engineering*, *9164*, 1–9. https://doi.org/10.1117/12.2061919

Meng, F., & Sachs, F. (2012). Orientation-based FRET sensor for real-time imaging of cellular forces. *Journal of Cell Science*, *125*(Pt 3), 743–50. https://doi.org/10.1242/jcs.093104

Meng, F., Suchyna, T. M., & Sachs, F. (2008). A fluorescence energy transfer-based mechanical stress sensor for specific proteins in situ. *FEBS Journal*, *275*(12), 3072–3087. https://doi.org/10.1111/j.1742-4658.2008.06461.x

Mizuno, D., Tardin, C., Schmidt, C. F., & MacKintosh, F. C. (2007). Nonequilibrium Mechanics of Active Cytoskeletal Networks. *Science*, *315*(5810). Retrieved from http://science.sciencemag.org/content/315/5810/370

Nicholas, M. P., Höök, P., Brenner, S., Wynne, C. L., Vallee, R. B., & Gennerich, A. (2015). Control of cytoplasmic dynein force production and processivity by its C-terminal domain. *Nature Communications*, *6*, 6206. https://doi.org/10.1038/ncomms7206

Okada, Y., & Hirokawa, N. (1999). A Processive Single-Headed Motor: Kinesin Superfamily Protein KIF1A. *Science (New York, N.Y.)*, *283*(5405), 1152–1157. https://doi.org/10.1126/science.283.5405.1152

Okada, Y., Sato-Yoshitake, R., & Hirokawa, N. (1995). The activation of protein kinase A pathway selectively inhibits anterograde axonal transport of vesicles but not mitochondria transport or retrograde transport in vivo. *Journal of Neuroscience*, *15*(4).

Polacheck, W. J., & Chen, C. S. (2016). Measuring cell-generated forces: a guide to the available tools. *Nature Methods*, *13*(5), 415–423. https://doi.org/10.1038/nmeth.3834

Rai, A. K., Rai, A., Ramaiya, A. J., Jha, R., & Mallik, R. (2013). Molecular Adaptations Allow Dynein to Generate Large Collective Forces inside Cells. *Cell*, *152*(1), 172–182. https://doi.org/10.1016/j.cell.2012.11.044

Rasband, W. S. (1997). Image J. Retrieved from http://imiagej.nih.gov/ij/

Reis, G. F., Yang, G., Szpankowski, L., Weaver, C., Shah, S. B., Robinson, J. T., … Goldstein, L. S. B. (2012). Molecular motor function in axonal transport in vivo probed by genetic and computational analysis in Drosophila. *Molecular Biology of the Cell*, *23*(9), 1700–1714. https://doi.org/10.1091/mbc.E11-11-0938

Schnitzer, M. J., & Block, S. M. (1997). Kinesin hydrolyses one ATP per 8-nm step. *Nature*, *388*(6640), 386–390. https://doi.org/10.1038/41111

Schnitzer, M. J., Visscher, K., & Block, S. M. (2000). Force production by single kinesin motors. *Nature Cell Biology*, *2*(10), 718–23. https://doi.org/10.1038/35036345

Seifert, U. (2005). Entropy Production along a Stochastic Trajectory and an Integral Fluctuation Theorem. *Physical Review Letters*, *95*(4), 40602. https://doi.org/10.1103/PhysRevLett.95.040602

Shubeita, G. T. G. T., Tran, S. L., Xu, J., Vershinin, M., Cermelli, S., Cotton, S. L., … Wieschaus, E. F. (2008). Consequences of Motor Copy Number on the Intracellular Transport of Kinesin-1-Driven Lipid Droplets. *Cell*, *135*(6), 1098–1107. https://doi.org/10.1016/j.cell.2008.10.021

Toba, S., Watanabe, T. M., Yamaguchi-Okimoto, L., Toyoshima, Y. Y., & Higuchi, H. (2006). Overlapping hand-over-hand mechanism of single molecular motility of cytoplasmic dynein. *Proceedings of the National Academy of Sciences*, *103*(15), 5741–5745. https://doi.org/10.1073/pnas.0508511103

Torisawa, T., Ichikawa, M., Furuta, A., Saito, K., Oiwa, K., Kojima, H., … Furuta, K. (2014). Autoinhibition and cooperative activation mechanisms of cytoplasmic dynein. *Nature Cell Biology*, *16*(11), 1118–1124. https://doi.org/10.1038/ncb3048

Turlier, H., Fedosov, D. A., Audoly, B., Auth, T., Gov, N. S., Sykes, C., … Betz, T. (2016). Equilibrium physics breakdown reveals the active nature of red blood cell flickering. *Nature Physics*, *12*(5), 513–519. https://doi.org/10.1038/nphys3621

Wirtz, D. (2009). Particle-Tracking Microrheology of Living Cells: Principles and Applications. *Annual Review of Biophysics*, *38*(1), 301–326. https://doi.org/10.1146/annurev.biophys.050708.133724

Yajima, H., Ogura, T., Nitta, R., Okada, Y., Sato, C., & Hirokawa, N. (2012). Conformational changes in tubulin in GMPCPP and GDP-taxol microtubules observed by cryoelectron microscopy. *The Journal of Cell Biology*, *198*(3), 315–22. https://doi.org/10.1083/jcb.201201161

Zimmermann, E., & Seifert, U. (2012). Efficiencies of a molecular motor: a generic hybrid model applied to the F_1-ATPase. *New Journal of Physics*, *14*(10), 103023. https://doi.org/10.1088/1367-2630/14/10/103023

Acknowledgments

We thank N. Sawairi and M. Tomishige for initial stages of experiments; S. Xu, J. Asada, M. Komeno, M. Kakiuchi and K. Ito for their technical and secretarial assistance; W. Kylius for editing the manuscript.

Figures

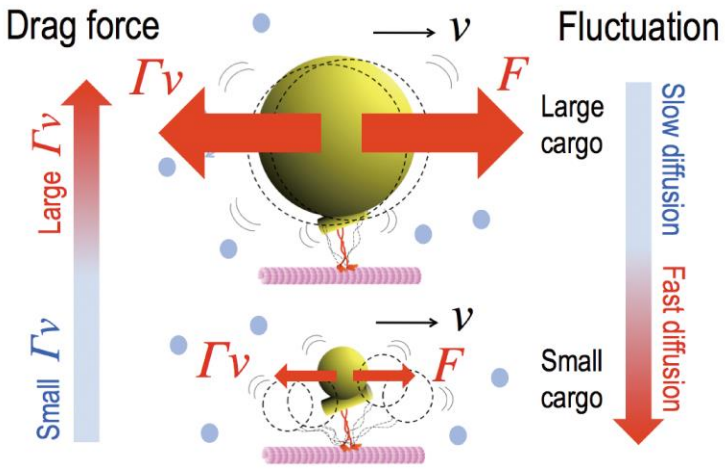

Figure 1. Schematics of the theoretical idea of FT.

Force (F) exerted by motors (red) along a microtubule (pink) is balanced by the drag force (Γv) where Γ is the friction coefficient of a cargo (yellow). The dashed circles represent fluctuating movement of the cargo, and the blue circles represent water molecules or vesicles that collide with the cargo. When the viscosity effect acting on a cargo is large (top), the fluctuation of a cargo's position becomes small and the drag force becomes large, and *vice versa* (bottom). The inverse relation between F and fluctuation suggests the possibility that F is inferred from the fluctuation.

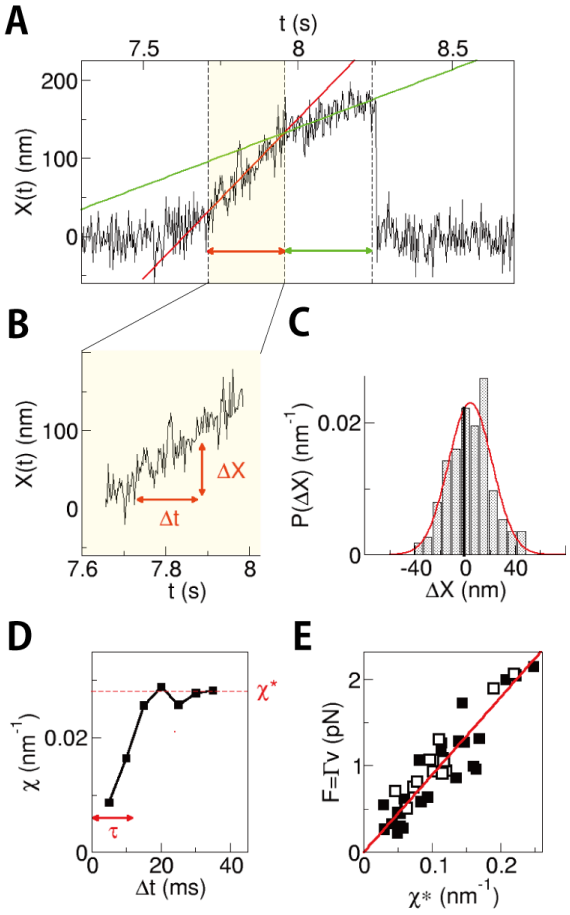

Figure 2. Proof-of-principle experiments: force measurement of kinesin-driven bead under optical tweezers.

(A) An example of the trace of the bead's displacement $X(t)$ obtained in the *in vitro* experiment using an optical tweezers instrument. The bead was carried by kinesin motors along a microtubule under the load by the optical tweezers. Segments for the analysis in the graph indicated with red and green were determined by fitting the trajectory to the constant velocity movement as detailed in the Methods section. **(B)** Analysis of fluctuation. The fluctuation was calculated as $\Delta X=X(t+\Delta t)-X(t)$. **(C)** Distribution of ΔX at Δt=30 ms fitted by a Gaussian function. **(D)** Relaxation of χ. χ^* and τ denote the value of convergence and the time constant, respectively. **(E)** The drag force estimated from the Stokes law ($F=\Gamma v$) is plotted against χ^* for the traces with the stall force < 12 pN (closed squares (n=29)) and > 12 pN (open squares (n=16)). The data points aligned linearly, confirming equation (1').

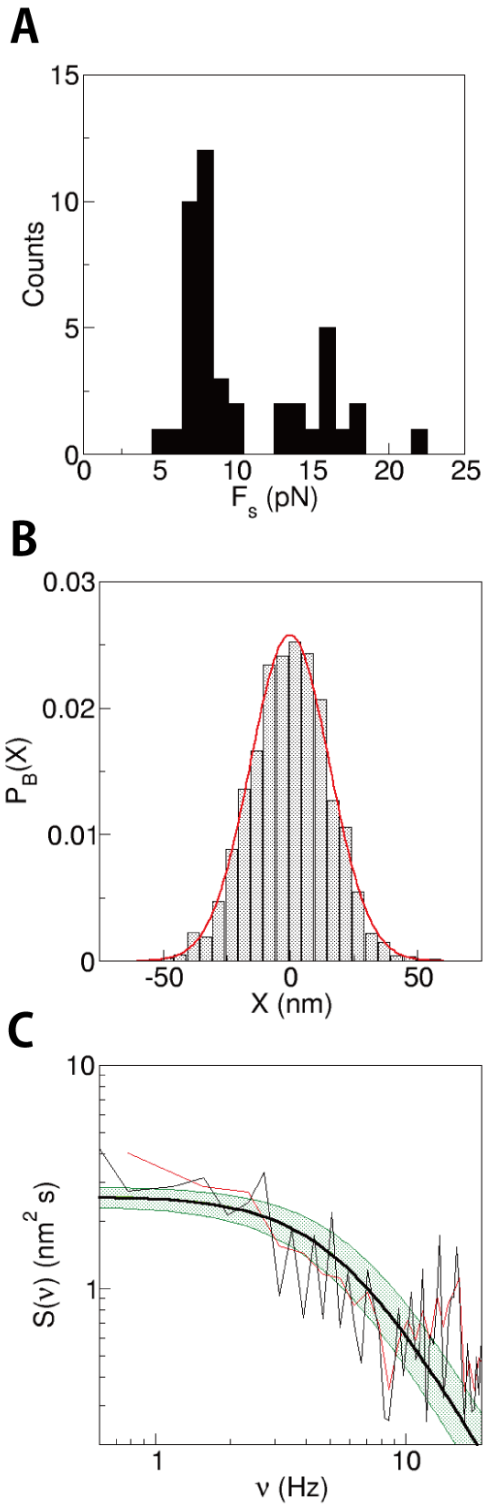

Figure 2 – figure supplement 1.

Detailed analysis of the movement of the kinesin-coated bead.

(A) Stall force (F_s) distribution of the kinesin-driven beads measured under optical tweezers (n=43). Most of the beads showed processive runs with stall force at around 8 pN and 16 pN. **(B)** The equilibrium probability distribution $P_B(X)$ was fitted with a Gaussian function, whose variance $\sigma^2 = k_B T/\kappa_{eff}$ gives the estimate of the effective stiffness κ_{eff}. **(C)** The power spectrum density $S(\nu)$ was fitted with a Lorentzian function (right), whose corner frequency $\nu_c = \kappa_{eff}/\Gamma$ gives the estimate of the friction coefficient. The black and red curves correspond to the window size N_w=1024 and N_w=512, respectively. The thick black curve is the fitting Lorentzian function. The fitting error was estimated to be 20% CV by bootstrapping method (green area). Note that this friction coefficient (2.9 ± 0.4 μN s/m (mean ± SEM, n=4)) was nearly 300 times larger than the viscous drag of the bead in water (10 nN s/m). It is consistent with the previously reported values of kinesin-coated beads moving along a microtubule (Bormuth et al., 2009; Okada & Hirokawa, 1999; Mark J. Schnitzer & Block, 1997). The exact source of this large friction coefficient is unclear. The so-called protein friction would be a good candidate as proposed previously (Bormuth et al., 2009).

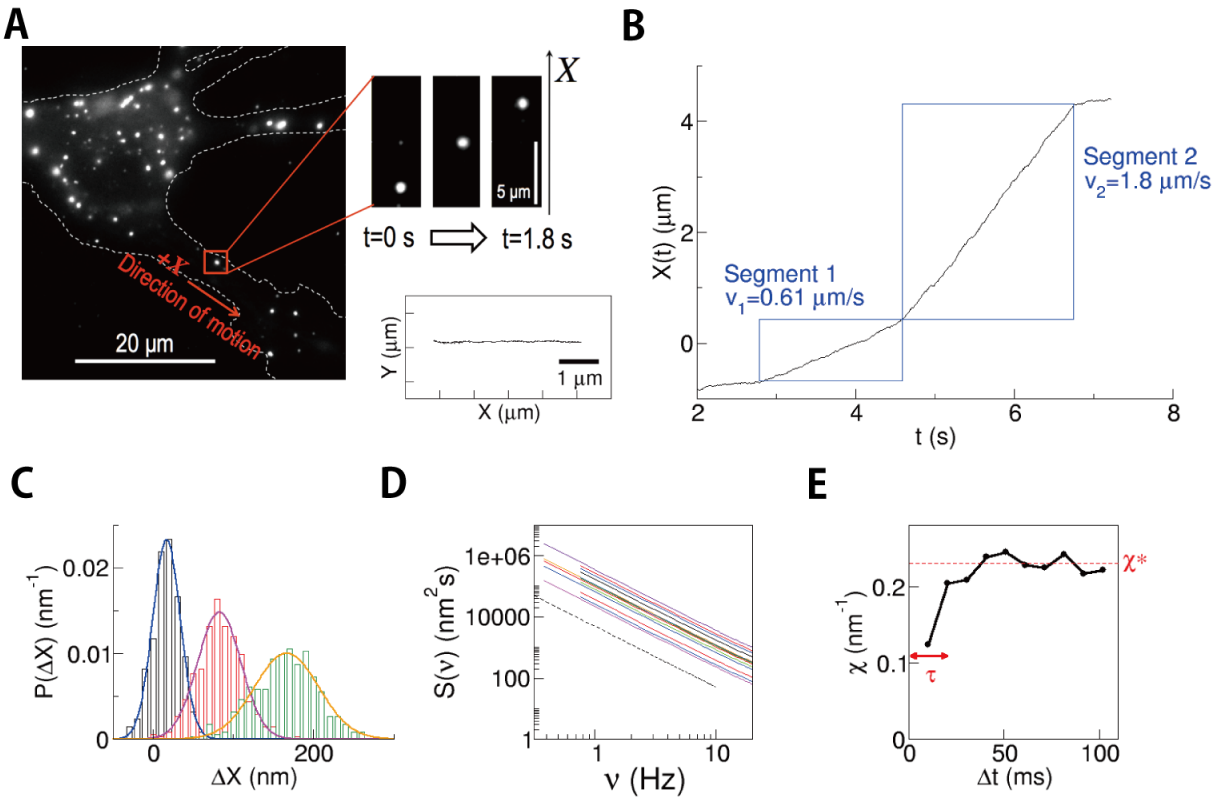

Figure 3. Measurement in the living neuron.

(A) A typical view of DiI-stained endosomes in a SCG neuron. In the right bottom panel, a typical 2D-trajectory of an endosome during 4 s is shown. **(B)** An example of the trace of the displacement $X(t)$ of an endosome, which showed a velocity change in the middle of the run event. The direction of movement was set as a plus direction of X. Segments for the analysis (rectangle areas) were determined by fitting the trajectory to the constant velocity movement as detailed in the Methods section. **(C)** Gaussian distribution of displacement $\Delta X=X(t+\Delta t)-X(t)$ in the cases Δt=10.2 ms (blue), 51.0 ms (pink), and 102 ms (green). (**D**) Power spectrum of the position $X(t)$ in a constant velocity segment inversely proportional to the square of the frequency (the dotted line with a slope of -2) (n=12), which is consistent with the assumption of white noise (supplementary text). **(E)** Relaxation of χ. χ^* and τ denote the value of convergence and the time constant, respectively. See also Figure 3–figure supplements 1, 2 for the detailed analysis of χ.

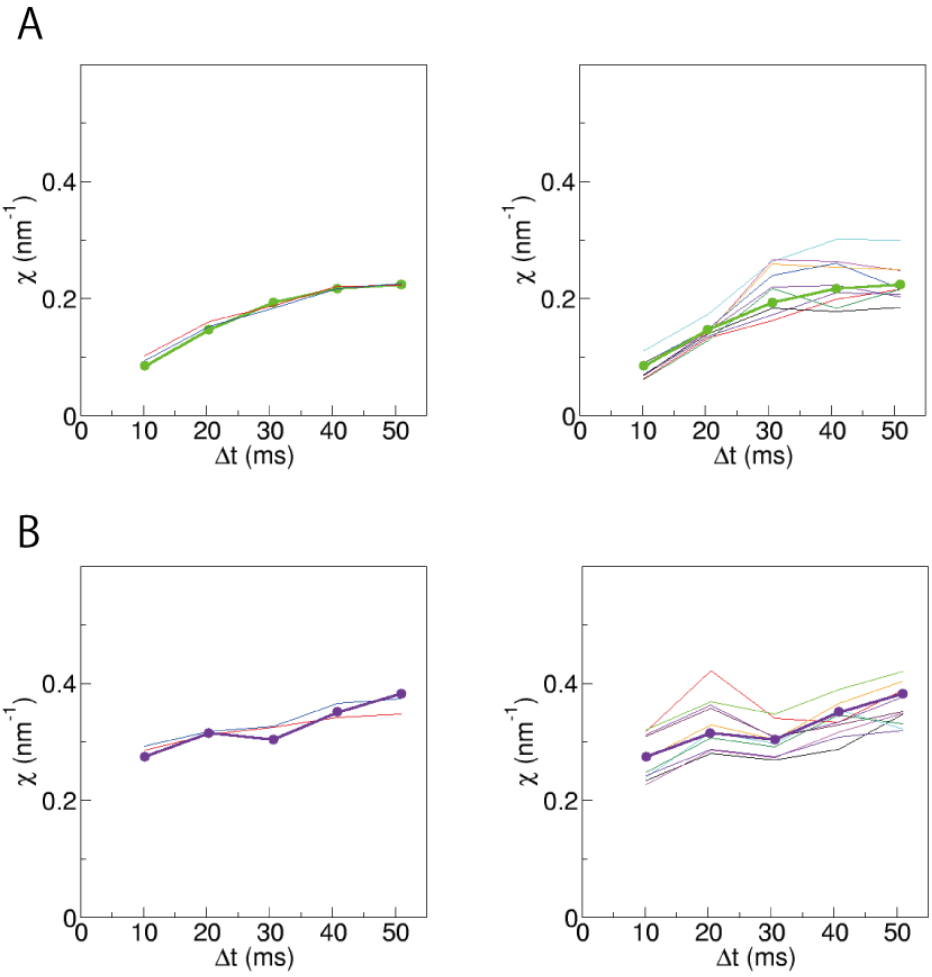

Figure 3 – figure supplement 1.

Evaluation of the errors in the estimation of the fluctuation *χ*.

Panels (**A**) and (**B**) represent an example of anterograde and retrograde vesicles, respectively. The left panels show the comparison of the method to estimate the Gaussian distribution from the observed ΔX values. The thick curves represent the estimation from the histogram of ΔX, which can be biased by binning. The thin blue curves are based on the fitting of the cumulative Gaussian distribution. The thin red curves show the results by simply calculating the average and the variance of ΔX, which can be biased by the tails of the distribution. The right panels show 10 sample results of the bootstrapping confirmation for the errors in the estimation. These bootstrapping results gave an estimate for the errors in the estimation of the fluctuation χ as 10% CV, which is consistent with the expected errors from the accuracy of the position measurement (8 nm).

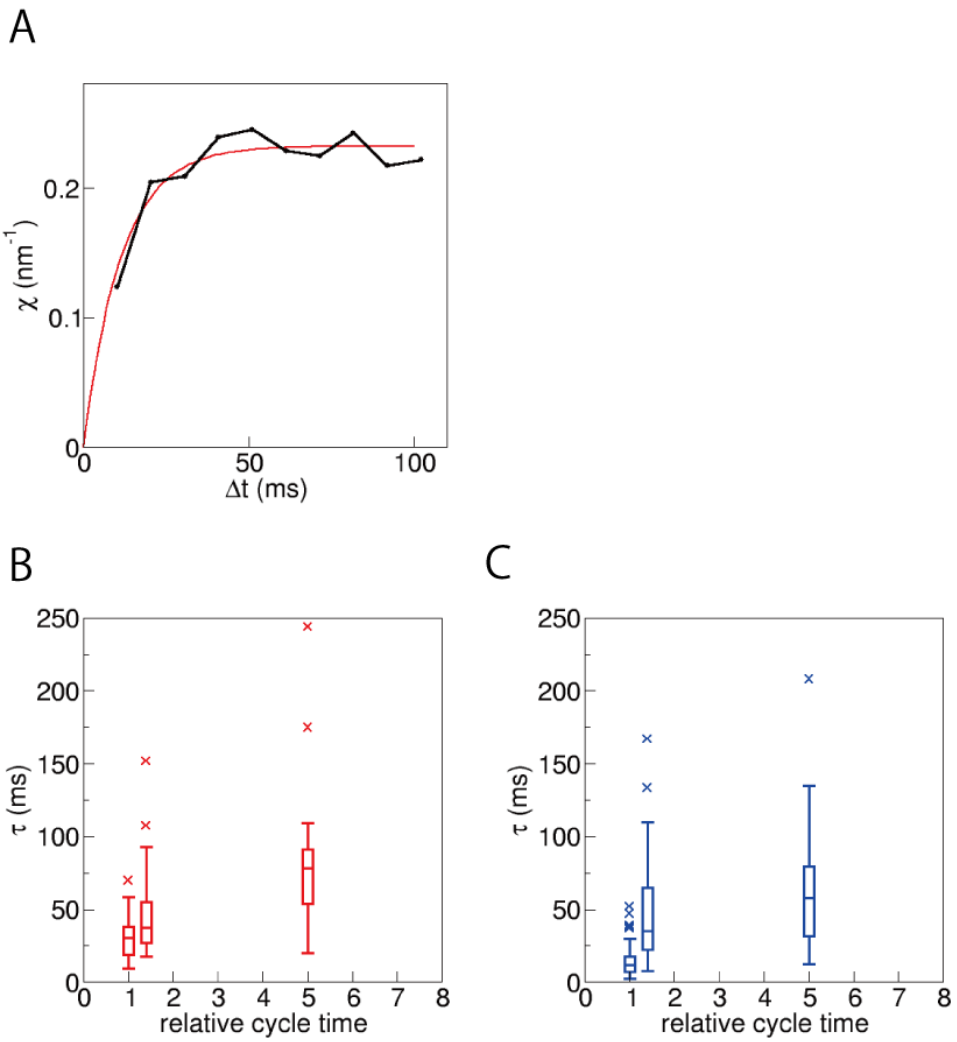

Figure 3 – figure supplement 2.

Analysis of the relaxation time.

(A) The relaxation time τ was estimated by fitting of the function $c(1-\exp(-\Delta t/\tau))$ to χ, where c is a constant. In this paper, the converged value of χ^* was calculated as χ at Δt=51 ms, noting that χ at Δt=51 ms is the same as c within the error of χ. **(B, C)** The fluctuation of the endosomes was analyzed in permeabilized and reactivated neurons, in which the ATP concentration was maintained at 125 μM and 12.5 μM. Both anterograde (B) and retrograde (C) endosomes showed slower relaxation when ATPase cycle was slowed down. The relative cycle time was calculated as $1+K_m/[ATP]$, where the Michaelis-Menten constant K_m was assumed to be 50 μM as an approximate value for both kinesin and dynein. The data are shown as box-and-whisker plots. 35 anterograde and 27 retrograde vesicles (from 29 and 24 cells) were analyzed for [ATP]=125 μM. 15 vesicles each (from 9 and 14 cells) for [ATP]=12.5μM.

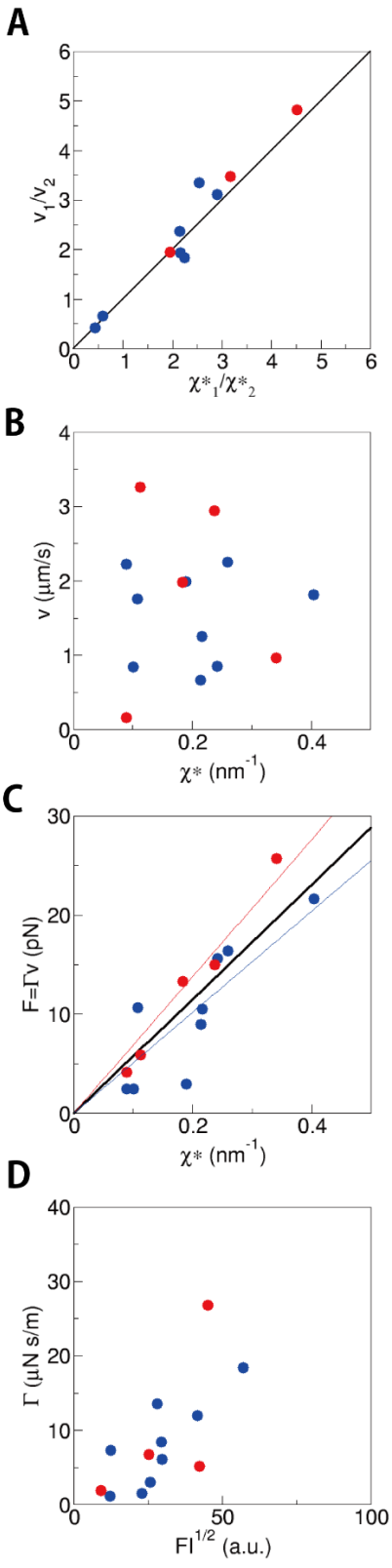

Figure 4. Validation of FT with axonal endosomes *in vivo*.

(A) Confirmation of the proportional relation between the velocity and the fluctuation (equation (3)) (n=3 for anterograde, n=7 for retrograde from > 200 traces). The traces with two successive constant velocity segments with different velocities v_1 and v_2 (see Figure 3B for example) were analyzed. (B-D) Analysis of endosomes (n=5 for anterograde (red), n=9 for retrograde from > 200 traces) which exhibited both constant velocity movement and pause (Figure 4–figure supplement 1) for the comparison of χ^* with $F(=\Gamma v)$. The friction coefficient (Γ) was estimated from the fluctuation during the pause. Although the plot of velocity (v) and χ^* is scattered in (B), the plot of Γv and χ^* shows a linear relation in (C), which is consistent with the fluctuation theorem equation (1'). The slope gives the effective temperature of the system T_{eff}, which was around 5000K for anterograde (red) and 3700K for retrograde (blue) endosomes. Because the difference was within the fitting error, we used 4200K as T_{eff} obtained from the black line for both endosomes. Γ showed a roughly linear correlation with the square root of fluorescence intensity (FI), with the correlation coefficient $R^2= 0.73$ in (D). This might be because the intensity of the fluorescent signal by a lipophilic dye DiI would be proportional to the surface area of the vesicle (insets of Figure 5C).

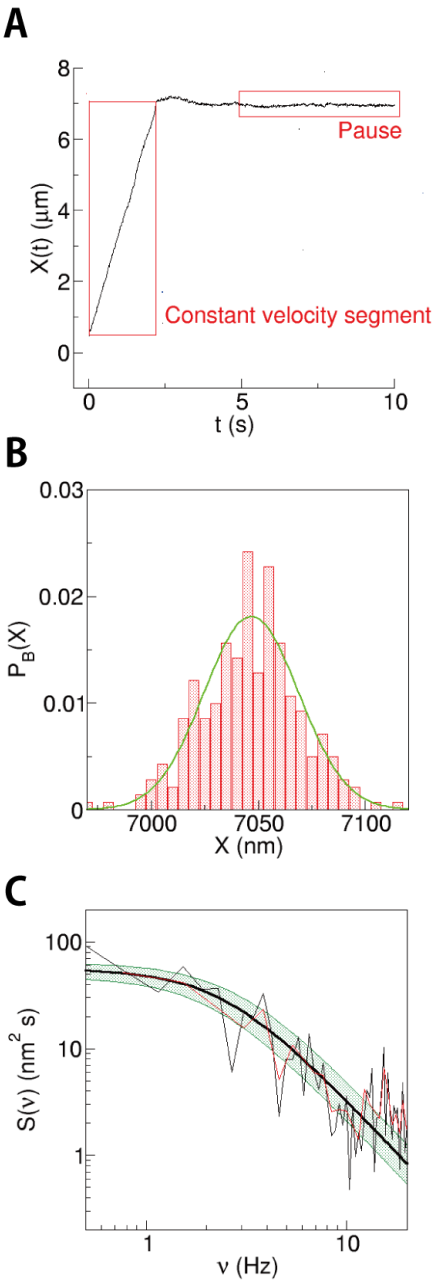

Figure 4 – figure supplement 1.

Estimation of the friction coefficient (Γ) from pausing endosomes in a neuron.

(A) An example of the traces for the analysis. The pausing segments just after the constant velocity run were analyzed. **(B)** The equilibrium probability distribution of the endosome position $P_B(X)$. The distribution was fitted with a Gaussian function, whose variance $\sigma^2 = k_B T/\kappa_{eff}$ gives the estimate for the effective stiffness κ_{eff}. **(C)** The power spectrum density $S(\nu)$. The spectrum was fitted with a Lorentzian function, whose corner frequency $\nu_c=\kappa_{eff}/\Gamma$ gives the estimate of the friction coefficient. The black and red curves correspond to the window size N_w=256 and N_w=128, respectively. The thick black curve is the fitting Lorentzian function. The fitting had error was estimated as 20% CV. The traces of 14 endosomes (from > 200 traces) which had both pausing segment and constant velocity segment were analyzed similarly, and the results are shown in Figure 4B-D.

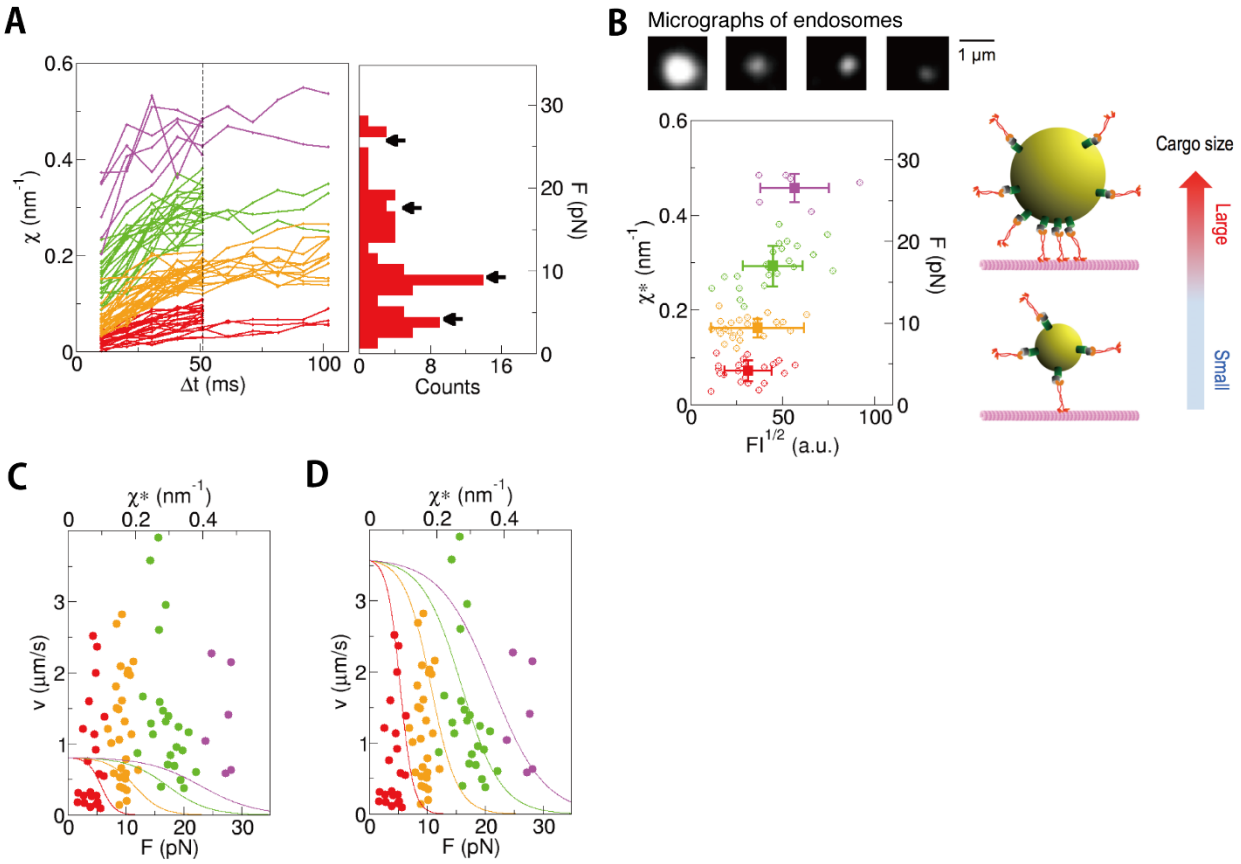

Figure 5. Measurement and analysis of the force for anterogradely transported endosomes in axon.

(A) The traces of χ plotted against Δt for anterograde endosomes (n=79). They were classified into four clusters by *k*-means clustering (indicated with different colors. See Methods for the details). The χ^* values (χ at Δt=51 ms) were converted to the force values by using the effective temperature T_{eff}= 4200K (Figure 4C) via equation (1'), and its distribution is shown as a histogram. The positions of the cluster centers are indicated by arrows. The source data files for this analysis are deposited to Systems Science of Biological Dynamics (SSBD) database (http://ssbd.qbic.riken.jp/set/20170801/). (B) The fluctuation χ^* (and the force) is plotted against the square root of fluorescence intensity (FI), which is a proxy for the radius of the endosome (Figure 4D). The color of each data point is the same as in the left panels in (A), which reflects the number of FPUs. The average and the SD for each cluster are shown with square symbols with error bars. There was a weak correlation between χ^* and $(FI)^{1/2}$ (R^2 =0.40), suggesting a tendency toward the larger endosomes experiencing a larger force with a greater number of force producing units (schema on the right side). (C) For each endosome, the velocity is plotted against

the force calculated by using the effective temperature T_{eff}= 4200K (Figure 4C). The curves are the results of *in vitro* measurements of kinesin-1 (M J Schnitzer et al., 2000). The four curves correspond to the number of kinesin-1 dimers =1, 2, 3 and 4. The colors for the data points are same as the panels in (A). (D) The data points (circles) are same as the panel (A). The curves for the anterograde endosomes are calculated using the same model as (C) but after adjustment of the maximum velocity (3.9 μm/s).

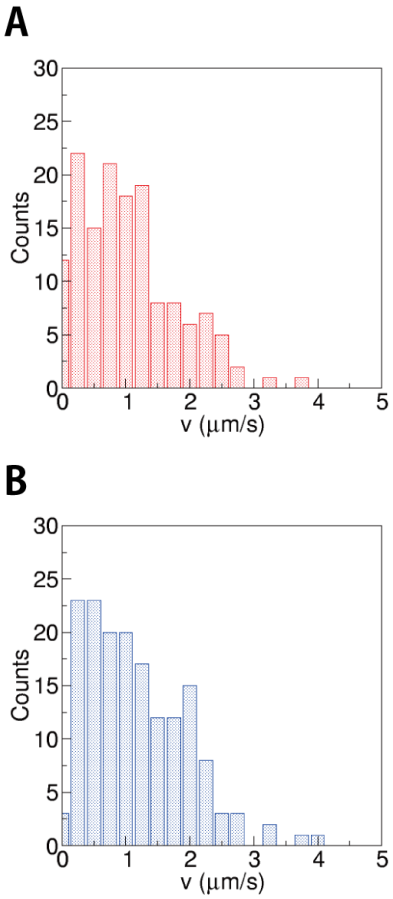

Figure 5 – figure supplement 1.

Velocity distributions of endosomes.

Velocity distributions of endosomes for anterograde transport **(A)** and retrograde transport **(B)**. Only the segments of constant velocity movement with durations longer than 2 s were analyzed (e.g. rectangles depicted in Figure 3B). The mean velocities were 1.2 ± 0.7 μm/s (mean ± SD, n=145) for anterograde transport, and 1.3 ± 0.8 μm/s (n=163) for retrograde transport, respectively. It should be noted that distinct peaks are not clear unlike the distributions of χ^* (Figure 5A, 6A).

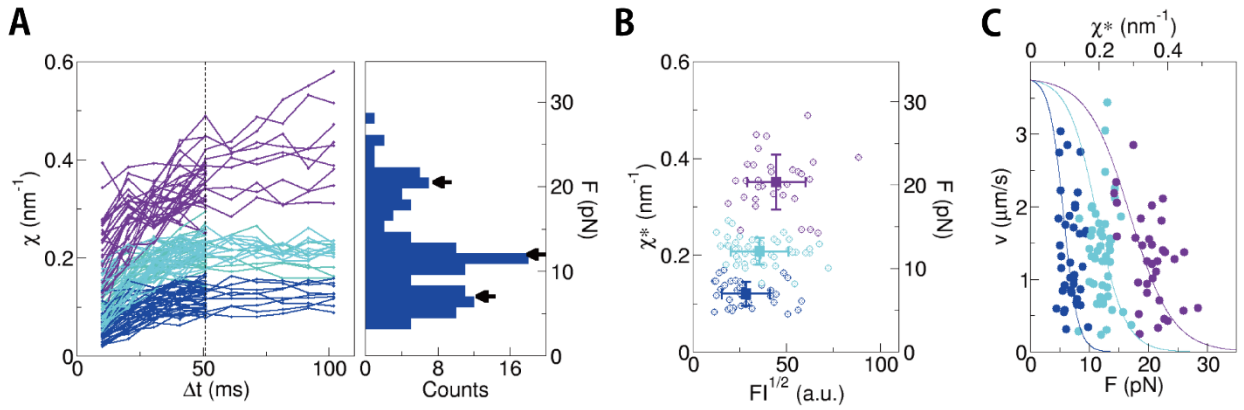

Figure 6. Measurement and analysis of the force for retrogradely transported endosomes in axon.

(A) The traces of χ plotted against Δt for anterograde endosomes (n=119). They were classified into three clusters by *k*-means clustering (indicated with different colors. See Methods for the details). The χ^* values (χ at Δt=51 ms) were converted to the force values by using the effective temperature T_{eff}= 4200K (Figure 4C) via equation (1'), and its distribution is shown as a histogram. The positions of the cluster centers are indicated by arrows. The source data files for this analysis are deposited to Systems Science of Biological Dynamics (SSBD) database (http://ssbd.qbic.riken.jp/set/20170801/). (B) The fluctuation χ^* (and the force) is plotted against the square root of fluorescence intensity (FI), which is a proxy for the radius of the endosome (Figure 4D). The color of each data point is the same as in the left panels in (A), which reflects the number of FPUs. The average and the SD for each cluster are shown with square symbols with error bars. There was a weak correlation between χ^* and $(FI)^{1/2}$ (R^2 =0.33), as observed with anterograde endosomes (Figure 5B). (C) The force-velocity relation was fitted with the same model equation for kinesin using the maximum force as the fitting parameter. The maximum velocity (4.1 μm/s) was determined from the measured value, and all other parameters were unchanged. The three curves correspond to the number of force producing units = 1, 2 and 3. The colors for the data points are same in other panels.

Supplemental Text for the Theory section

For the bead moving at a constant speed (v) *in vitro*, under highly damped conditions, the motion of center position $X(t)$ can be described by the Langevin equation:

$$\frac{dX(t)}{dt} = v + \sqrt{2D}\xi(t) \tag{S1}$$

where the second term on the right-hand side represents the stochastic collisions with solvent molecules, where ξ is Gaussian noise with $\langle \xi(t)\xi(t') \rangle = \delta(t-t')$, where < > denotes the time average over the time course, and D is a diffusion coefficient. It is well known, in near equilibrium, that D in equation (S1) satisfies the fluctuation-dissipation theorem (Howard, 2001), $D=k_BT/\gamma$ where γ is the friction coefficient of the bead, k_B is the Boltzmann constant, and T is the temperature of the environment. Using this relation, equation (1) is rewritten as

$$\gamma\frac{dX(t)}{dt} = F + \sqrt{2\gamma k_B T}\xi(t) \tag{S2}$$

where F is a force defined as $F=\gamma v$.

In the case of a cargo vesicle transport in cells, these relations cannot be applied directly. The cytoplasm in the living cell could be far from equilibrium and the fluctuation-dissipation theorem would be broken (Turlier et al., 2016). There can be more interactions between the vesicle with the surrounding environments than the simple collisions with solvents. The vesicles can be temporarily tethered to cytoskeletal filaments or interacting with other vesicles that are also driven by other molecular motors. Even in such complex situations, the friction force of the vesicle can be regarded to be proportional to the velocity unless the movement is too fast. This apparent friction coefficient Γ thus includes the interaction effect between the cargo and surrounding environment, so that it would be larger than $\gamma=6\pi\eta r$ as assumed in the classical Stokes formula (r: the radius of the cargo, η: the viscosity of the cytosol). This assumption was already examined experimentally by tracking the trajectories of the passive tracer beads in the cytoplasm (Wirtz, 2009).

Similarly, the second term on the right-hand side in equation (S2) should be revised. Since the assumption for Gaussian noise is based on the assumption that the noise is caused by large

numbers of independent interactions, it is not dependent on whether the system is close to the thermal equilibrium or not. In fact, the probability distribution of the fluctuation $\Delta X(t)$ measured in this study was Gaussian, and its power spectrum was inversely proportional to the square of the frequency (**Fig 3C, D**). These results experimentally confirmed the assumption of the white Gaussian noise. For the amplitude of the Gaussian noise, however, the fluctuation-dissipation theorem can no longer be assumed. Hence, we replace the equilibrium temperature T with an empirical parameter T_{eff}.

With these modifications, the movement of a vesicle in the cytoplasm can be modeled as (Figure 1)

$$\Gamma\frac{dX(t)}{dt} = F + \sqrt{2\gamma k_{\mathrm{B}}T_{\mathrm{eff}}}\,\xi(t) \tag{S3}$$

From the stochastic model (S3), the following fluctuation theorem is derived (Kumiko Hayashi et al., 2010):

$$\frac{F}{k_{\mathrm{B}}T_{\mathrm{eff}}} = \ln\left[P(\Delta X)/P(-\Delta X)\right]/\Delta X \tag{S4}$$

In this paper, the quantity on the right hand side is called as the degree of fluctuation χ:

$$\chi = \ln\left[P(\Delta X)/P(-\Delta X)\right]/\Delta X \tag{S5}$$

Then, equation (S5) becomes

$$\frac{F}{k_{\mathrm{B}}T_{\mathrm{eff}}} = \chi \tag{S6}$$

Here, it should be noted that equation (S3) is a phenomenological macroscopic model. Microscopically, the motion of the vesicle, for example, will be described by a more complex model like

$$\gamma\frac{dx}{dt} = -\frac{\partial U_{\mathrm{other}}(x,t)}{\partial x} - \frac{\partial U_{\mathrm{m}}(x,t)}{\partial x} + \sqrt{2\gamma k_{\mathrm{B}}T}\,\xi(t) \tag{S7}$$

where $\sqrt{2\gamma k_{\mathrm{B}}T}$ is thermal noise acting on the bead, U_{m} is an interaction between vesicle and motors, U_{other} is the other interactions acting on the vesicle. Equation (S3) corresponds to the coarse-grained model of equation (S7), and the microscopic effect of U_{m} and U_{other} contributes to the effective viscosity Γ, effective noise $\sqrt{2\gamma k_{\mathrm{B}}T_{\mathrm{eff}}}$ and the drag force F. Note that this decomposition of energy has been theoretically studied (Kumiko Hayashi & Sasa, 2005). Thus

the effective temperature T_{eff} is dependent on the microscopic hidden variables (Seifert, 2005; Zimmermann & Seifert, 2012).

Equation (S6) holds for the time scale long enough to be compared with the characteristic time scales for the microscopic interactions U_{m} and U_{other}, among which the enzymatic reaction of motor protein will be the slowest process with around 10 ms cycle time. Hence, the right-hand side of equation (S6), χ will show a relaxation behavior against the time interval Δt with the analysis for ΔX. The relaxation time constant τ is expected to show dependence on the cycle time of the motor protein, which was confirmed experimentally in the following sections. Therefore, equation (S6) is modified as follows to reflect that the converged value of χ^*, instead of the transient values of χ, should be used for the estimation of the drag force:

$$F = k_{\mathrm{B}} T_{\mathrm{eff}} \chi^* \tag{S8}$$